Supplement of

Maximum ozone concentrations in the southwestern US and Texas: Implications of the growing predominance of background ozone

David D. Parrish, Ian C. Faloona, and Richard G. Derwent

Correspondence to: David D. Parrish (david.d.parrish.llc@gmail.com)

Contents of this file

Introduction

This supporting information collects the parameter values derived from fits of Equations 3 and 4 to all ODV time series analyzed in this work in Tables S1 to S5. Figures S1 to S7 illustrate some of these fits and provide additional data presentations. Text S1 to S7 present additional discussion aspects of the observation-based model and model uncertainties.

Table S1. Parameter values (with 95% confidence limits) derived from fits of Equation 1 to time series of ODVs time series from the isolated rural CASTNET sites.

Site	*a* (ppb)	*b* (ppb yr^{-1})	*c* (ppb yr^{-2})	$year_{max}$	RMSD (ppb)
Glacier NP	54.9 ± 1.1	0.09 ± 0.16	-0.010 ± 0.011	2004 ± 9	1.2
Yellowstone NP	65.9 ± 2.9	-0.31 ± 0.67	+0.007 ± 0.032	---	1.7
Craters of the Moon NM	62.5 ± 3.8	0.16 ± 0.67	-0.009 ± 0.038	2009 ± 51	2.4
Lassen Volcanic NP	72.4 ± 2.7	-0.05 ± 0.35	-0.016 ± 0.025	1999 ± 11	3.1
Great Basin NP	71.5 ± 2.1	0.14 ± 0.51	-0.020 ± 0.028	2004 ± 13	2.0
Canyonlands NP	70.3 ± 2.0	0.17 ± 0.46	-0.024 ± 0.024	2003 ± 10	1.7
Grand Canyon NP	72.5 ± 1.3	0.07 ± 0.21	-0.026 ± 0.014	2001 ± 4	1.4
Chiricahua NM	70.1 ± 1.7	0.19 ± 0.29	-0.020 ± 0.018	2005 ± 8	1.8
All sites	67.7 ± 1.9	0.09 ± 0.33	-0.018 ± 0.020	2003 ± 10	5.9
All sites - normalized	71.3 ± 0.8	0.07 ± 0.13	-0.015 ± 0.008	2002 ± 4	2.4

Table S2. Parameter values from fits of Equation 3 to time series of percentiles of maximum MDA8 ozone concentration distributions recorded in the California air basins and calculated from the ozone sondes launched from Trinidad Head CA. RMSD gives the root-mean-square deviations between the observed ozone concentrations and the derived fits.

Data set	***a*** (ppb)	***A*** (ppb)	**RMSD** (ppb)
Maximum			
San Diego AB	52.6 ± 13.4	58.6 ± 9.7	16.8
SoCAB	66.6 ± 13.4	95.8 ± 9.7	16.7
SFB AB	75.5 ± 9.6	25.1 ± 6.9	11.9
North Coast AB	65.4 ± 7.7	4.6 ± 6.0	12.0
Ozone sondes	76.5	---	---
98th percentile			
San Diego AB	58.6 ± 5.7	41.0 ± 4.1	7.1
SoCAB	60.8 ± 8.9	87.7 ± 6.4	11.1
SFB AB	70.2 ± 6.5	21.1 ± 4.7	8.0
North Coast AB	58.1 ± 5.7	4.3 ± 4.5	8.9
Ozone sondes	76.5	---	---
90th percentile			
San Diego AB	54.2 ± 3.5	32.5 ± 2.5	4.4
SoCAB	53.0 ± 5.6	76.6 ± 4.1	7.0
SFB AB	54.8 ± 5.1	18.5 ± 3.7	6.3
North Coast AB	47.6 ± 3.9	4.1 ± 3.0	6.1
Ozone sondes	52.3	---	---
75th percentile			
San Diego AB	49.5 ± 2.9	27.9 ± 2.1	3.7
SoCAB	50.0 ± 5.7	65.0 ± 4.1	7.1
SFB AB	45.6 ± 3.5	14.4 ± 2.5	4.3
North Coast AB	42.4 ± 3.2	3.0 ± 2.5	5.0
Ozone sondes	45.8	---	---
median			
San Diego AB	45.8 ± 3.0	21.5 ± 2.2	3.7
SoCAB	46.4 ± 5.9	50.8 ± 4.3	7.4
SFB AB	38.8 ± 2.8	10.9 ± 2.0	3.5
North Coast AB	37.6 ± 2.7	1.3 ± 2.1	4.2
Ozone sondes	39.3	---	---
25th percentile			
San Diego AB	43.2 ± 3.2	14.9 ± 2.3	4.0
SoCAB	45.6 ± 7.1	34.4 ± 5.1	8.8
SFB AB	33.8 ± 2.1	8.6 ± 1.5	2.6
North Coast AB	33.1 ± 2.7	0.5 ± 2.1	4.2
Ozone sondes	31.8	---	---
10th percentile			
San Diego AB	40.4 ± 2.8	10.1 ± 2.0	3.5
SoCAB	46.1 ± 6.9	18.0 ± 5.0	8.6
SFB AB	29.1 ± 2.0	7.7 ± 1.4	2.5
North Coast AB	29.3 ± 2.4	-0.7 ± 1.9	3.7
Ozone sondes	25.7	---	---
Minimum			
San Diego AB	31.5 ± 4.1	4.4 ± 3.2	6.4
SoCAB	43.1 ± 4.4	0.1 ± 3.4	6.9
SFB AB	22.7 ± 3.0	5.2 ± 2.4	4.7
North Coast AB	20.7 ± 3.3	-2.8 ± 2.6	5.1
Ozone sondes	5.8	---	---

Table S3. Parameter values from all fits of Equation 3 to time series of ODVs recorded in the southwestern US. RMSD gives the root-mean-square deviations between the observed ODVs and the derived fits.

Site(s)	*a* (ppb)	*A* (ppb)	Npts[a]	RMSD (ppb)	years
CASTNET					
CASTNET - normalized	68.5 ± 1.5	2.8 ± 1.9	212	2.3	1990-2021
Southwestern US - rural					
AZ rural	66.6 ± 1.9	5.4 ± 2.5	116	2.3	1990-2021
Southern UT, Mesquite NV	64.8 ± 3.6	6.5 ± 5.6	66	2.6	1995-2021
Four Corners area rural	69.6 ± 4.3	-2.7 ± 6.6	126	4.0	1996-2021
Southern NM rural	69.4 ± 5.5	-1.3 ± 8.0	76	4.7	1992-2021
CO rural	69.0 ± 3.1	-1.9 ± 4.4	97	4.0	1986-2021
Southwestern US - urban					
Phoenix	69.0 ± 1.7	9.4 ± 2.3	658	4.8	1990-2021
Phoenix max	75.2 ± 4.9	10.2 ± 5.4	32	2.9	1990-2021
Tucson	63.9 ± 1.4	7.5 ± 1.2	264	3.4	1975-2021
Tucson max	66.2 ± 2.9	9.7 ± 2.4	38	2.3	1980-2021
Las Vegas	68.0 ± 2.6	11.6 ± 3.8	230	3.1	2000-2021
Las Vegas max	69.6 ± 6.6	15.4 ± 9.9	22	2.3	2000-2021
Reno	66.3 ± 2.2	4.9 ± 2.4	169	3.8	1982-2021
Reno max	67.1 ± 4.8	6.8 ± 4.1	39	3.8	1982-2021
Salt Lake City	66.6 ± 1.9	11.8 ± 1.7	351	5.2	1977-2021
Salt Lake City max	68.9 ± 4.3	15.0 ± 3.2	43	3.8	1979-2021
Albuquerque-Santa Fe	66.2 ± 1.8	4.0 ± 1.7	275	3.8	1981-2021
Albuquerque-Santa Fe max	68.4 ± 3.0	5.3 ± 2.4	41	2.5	1981-2021
Denver	69.0 ± 2.1	8.0 ± 1.7	412	6.2	1974-2021
Denver max	74.7 ± 2.1	9.4 ± 1.4	47	4.3	1974-2021

[a] Npts gives the number of ODVs included in each fit

Table S4. Parameter values from fits of Equation 4 to time series of maximum ODVs recorded in southwestern US, Texas and two other urban areas, TX, New York City, with the *a* parameter held at that derived for all ODVs in the respective urban area. RMSD gives the root-mean-square deviations between the observed maximum ODVs and the derived fits.

Site(s)	*a* (ppb)	A_{WF} (ppb)	*WF* (ppb)	RMSD (ppb)	years
Southwestern US - urban					
Phoenix max	69.0	12.9 ± 3.6	1.6 ± 2.5	3.0	1990-2021
Tucson max	63.9	10.5 ± 1.6	1.4 ± 1.6	2.2	1980-2021
Las Vegas max	68.0	16.1 ± 6.6	0.8 ± 3.3	1.8	2000-2021
Reno max	66.3	7.0 ± 1.3	0.6 ± 1.4	3.8	1982-2021
Salt Lake City max	66.6	15.6 ± 2.0	1.6 ± 2.5	3.7	1977-2021
Albuquerque-Santa Fe max	66.2	6.0 ± 1.5	1.4 ± 1.7	2.5	1981-2021
Denver max	69.0	11.0 ± 1.7	4.0 ± 2.5	4.0	1974-2021
Other urban areas					
Houston max	53.9	54.4 ± 3.2	1.8 ± 2.0	3.6	1995-2021
Dallas max	57.7	43.0 ± 2.5	2.6 ± 1.2	1.7	2000-2021
El Paso max	64.6	14.2 ± 2.1	3.2 ± 2.8	4.3	1977-2021
New York City max	52.2	39.7 ± 2.3	3.1 ± 1.2	3.7	2000-2021
Atlanta max	49.1	54.4 ± 9.9	1.2 ± 6.1	5.4	1995-2021

Table S5. Parameter values from all fits of Equation 3 to time series of ODVs recorded in nine Texas regions and neighboring states. RMSD gives the root-mean-square deviations between the observed ODVs and the derived fits.

Site(s)	*a* (ppb)	*A* (ppb)	Npts[a]	RMSD (ppb)	years
CASTNET					
CASTNET - normalized	68.5 ± 1.5	2.8 ± 1.9	212	2.3	1990-2021
Texas Regions					
Dallas region	57.7 ± 3.1	34.6 ± 4.5	422	5.9	1995-2021
Houston region	53.9 ± 3.2	43.2 ± 4.2	478	6.7	1995-2021
El Paso region	64.6 ± 1.8	11.5 ± 1.7	366	4.9	1976-2021
San Antonio region	58.4 ± 4.1	26.6 ± 6.3	138	3.9	2000-2021
Beaumont-PA-LC	54.7 ± 3.4	28.0 ± 5.1	230	4.0	2000-2021
So Coast Texas	52.1 ± 4.1	27.5 ± 6.0	63	2.5	2000-2021
SW Texas	49.8 ± 4.9	18.2 ± 6.9	72	3.1	2000-2021
Tyler-LV-SP	50.8 ± 4.6	37.3 ± 6.8	89	3.5	2000-2021
Western rural region	64.9 ± 5.8	3.2 ± 8.1	50	3.5	1989-2017
Other Western States					
Oklahoma	56.6 ± 2.8	25.1 ± 4.4	365	4.0	2000-2021
Louisiana	54.3 ± 2.3	29.9 ± 3.3	519	4.2	2000-2021
Arkansas	48.2 ± 4.7	37.5 ± 7.6	141	4.5	2000-2021
Kansas	56.6 ± 4.2	20.2 ± 6.6	174	4.3	2000-2021
Nebraska	56.5 ± 4.0	7.4 ± 3.6	146	6.6	1980-2021
Montana	58.6 ± 1.6	1.25[b]	99	4.7	1979-2021
North Dakota	59.6 ± 0.9	1.25[b]	181	3.6	1982-2021
South Dakota	62.2 ± 1.7	1.25[b]	80	4.4	1990-2021
Wyoming	64.2 ± 0.6	1.25[b]	227	2.8	1999-2021

[a] Npts gives the number of ODVs included in each fit

[b] Fit with *A* parameter value held fixed at this value

Table S6. Two-letter state abbreviations

State		State		State	
Alabama	AL	Kentucky	KY	North Dakota	ND
Alaska	AK	Louisiana	LA	Ohio	OH
Arizona	AZ	Maine	ME	Oklahoma	OK
Arkansas	AR	Maryland	MD	Oregon	OR
California	CA	Massachusetts	MA	Pennsylvania	PA
Colorado	CO	Michigan	MI	Rhode Island	RI
Connecticut	CT	Minnesota	MN	South Carolina	SC
Delaware	DE	Mississippi	MS	South Dakota	SD
District of Columbia	DC	Missouri	MO	Tennessee	TN
Florida	FL	Montana	MT	Texas	TX
Georgia	GA	Nebraska	NE	Utah	UT
Hawaii	HI	Nevada	NV	Vermont	VT
Idaho	ID	New Hampshire	NH	Virginia	VA
Illinois	IL	New Jersey	NJ	Washington	WA
Indiana	IN	New Mexico	NM	West Virginia	WV
Iowa	IA	New York	NY	Wisconsin	WI
Kansas	KS	North Carolina	NC	Wyoming	WY

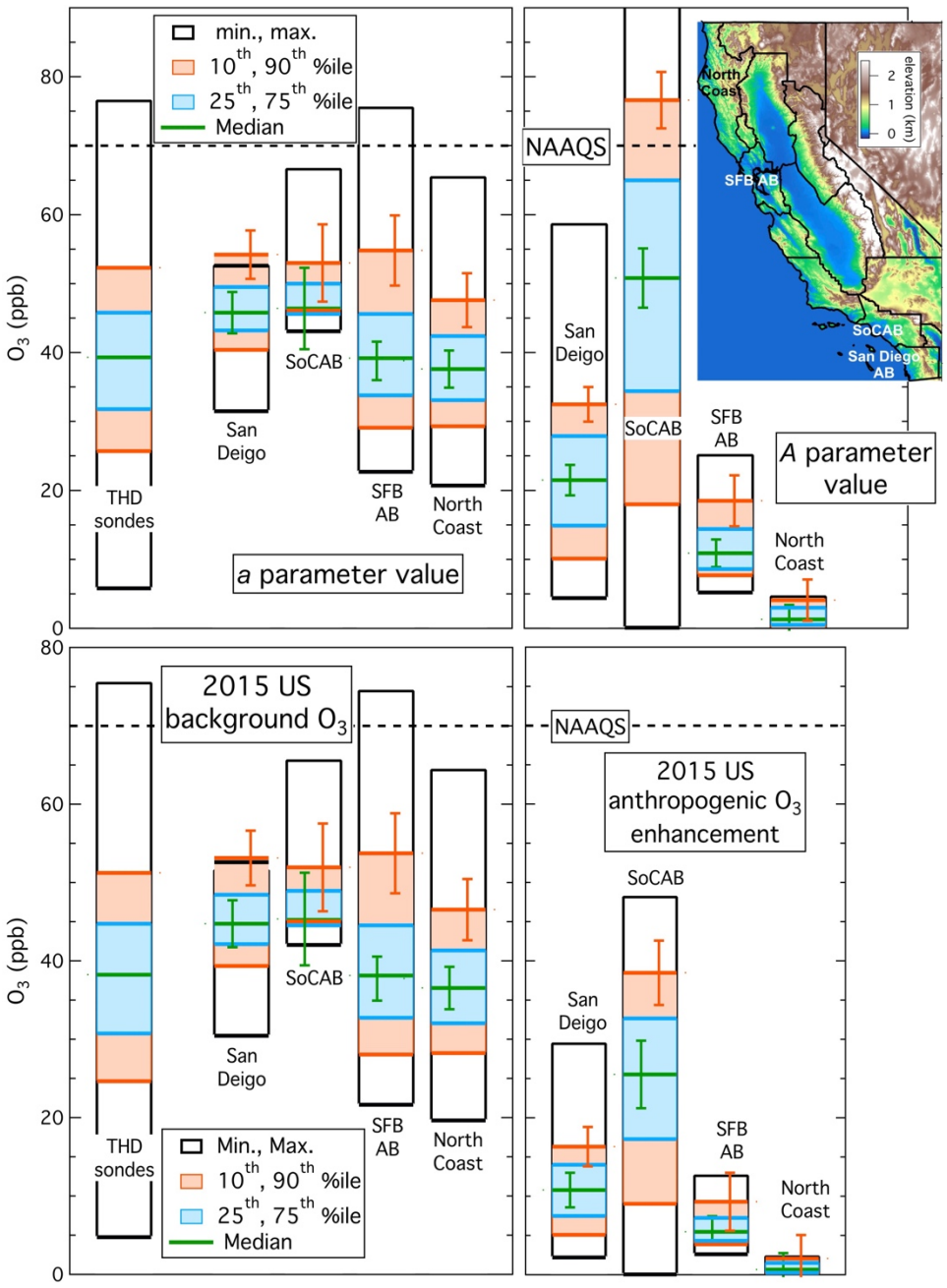

Figure S1. Comparison of distribution of ozone concentrations measured between 0.6 and 1 km altitude by sondes launched from Trinidad Head from May through September, 1997-2017 (left bar in two left graphs) and distributions of **(top)** *a* and *A* parameter values and (**bottom**) year 2015 US background ozone contribution and US anthropogenic ozone enhancement derived from the temporal evolution of maximum MDA8 ozone concentrations measured in 4 coastal California air basins. Figure 2 of the manuscript illustrates that MDA8 evolution. Error bars on the median and 90th percentile lines indicate estimated uncertainties. The inset map identifies the 4 air basins, with the black lines indicating the air basin boundaries.

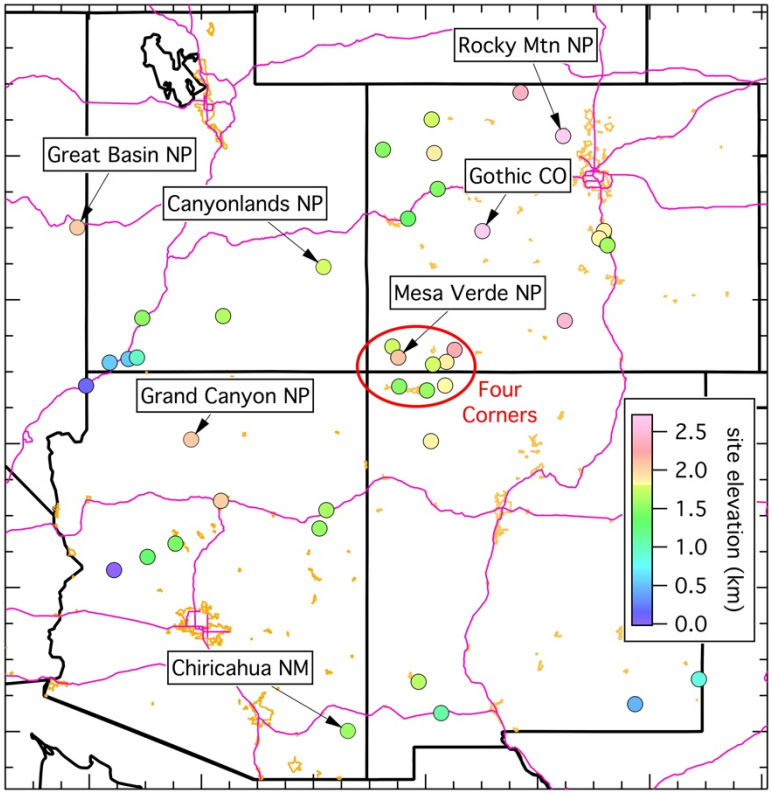

Figure S2. Map of southwestern US rural monitoring sites; the symbols are color-coded according to site elevation as annotated. Lines indicate outlines of southwestern US states (black), urban areas (gold) and interstates and selected other major highways (violet). ODV time series from rural areas whose sites are analyzed together as separate data sets are included in Figure S3. Locations of specific CASTNET sites as well as the Four Corners area are annotated.

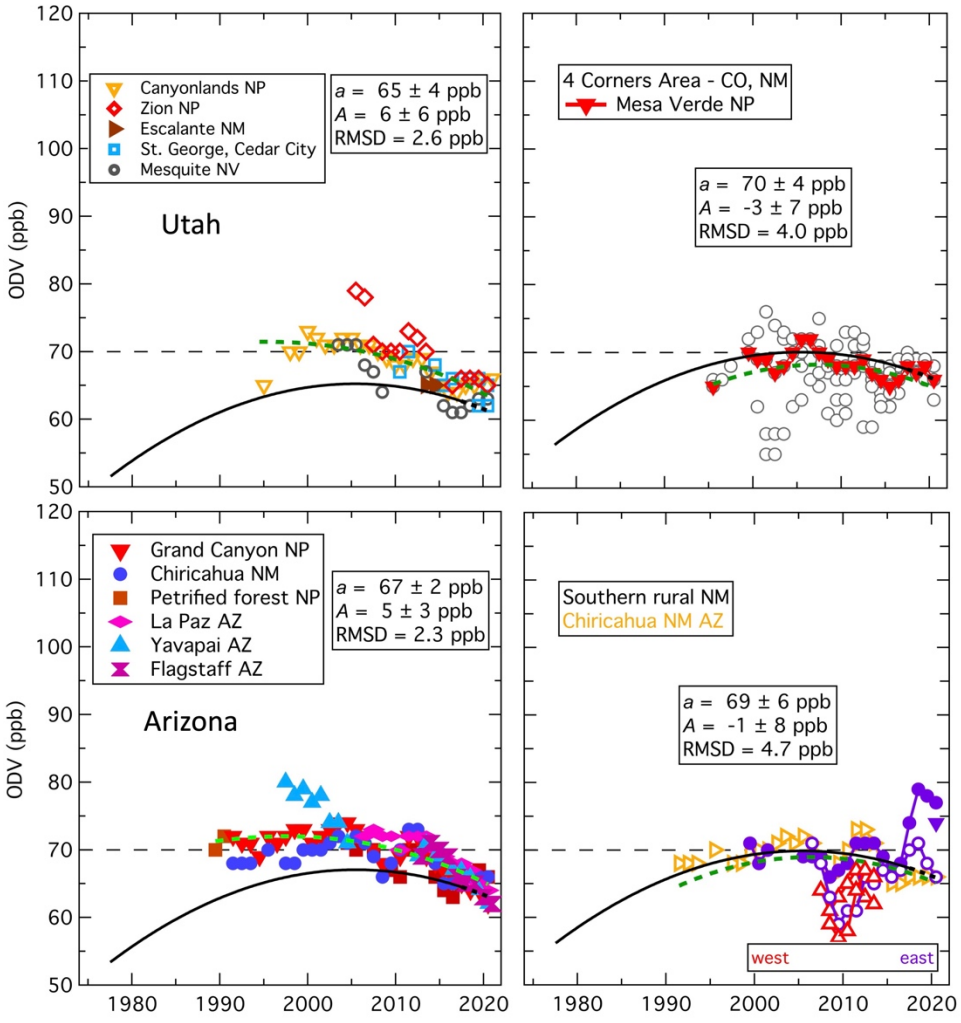

Figure S3. Time series of ODVs recorded in four southwestern US rural areas shown in Figure S2. Symbols indicate different sites as annotated. The southern NM sites are identified as western and eastern by different colors. Green dashed curves indicate fits of Equation 3 to all ODVs, with the parameters derived in the fit annotated. The black solid curves with dashed extensions indicate the fit to the baseline data from Figure 1, normalized to the respective *a* parameter values. The light dashed lines indicate the 70 ppb ozone NAAQS.

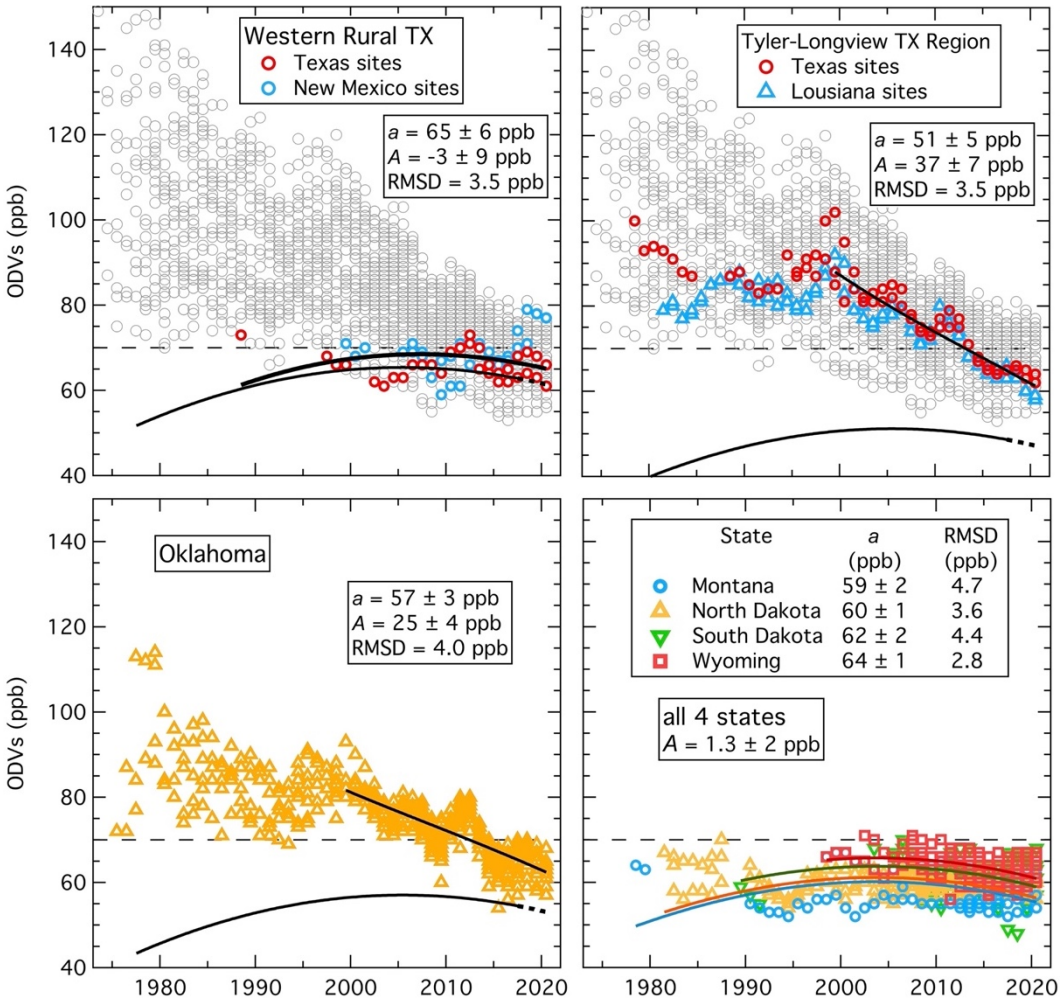

Figure S4. **(upper graphs)** Time series of ODVs recorded in two of the Texas regions shown in Figure 7 of the manuscript. Grey symbols in each graph indicate all recorded Texas ODVs. Colored symbols indicate the ODVs from each respective area. Upper curves indicate fits of Equation 3 to all ODVs in the area; the parameters derived in these fits are annotated. Lower curves with dashed extensions indicate the fit to the baseline data from Figure 1, but here normalized to the respective *a* parameter values. **(lower graphs)** Time series of ODVs recorded in Oklahoma and the four northern rural states. For Oklahoma upper curve indicates fit of Equation 3 to all ODVs in the state for 2000-2021; the parameters derived in this fit is annotated. Lower curve with dashed extension indicates the fit to the baseline data from Figure 1, normalized to the *a* parameter value derived for Oklahoma.For the northern states the curves indicate fits of Equation 3 to all ODVs recorded in each state; in these fits the *A* parameter value is fixed at 1.25 ppb. The derived *a* parameter values are annotated. In all graphs, the light dashed lines indicate the 70 ppb ozone NAAQS.

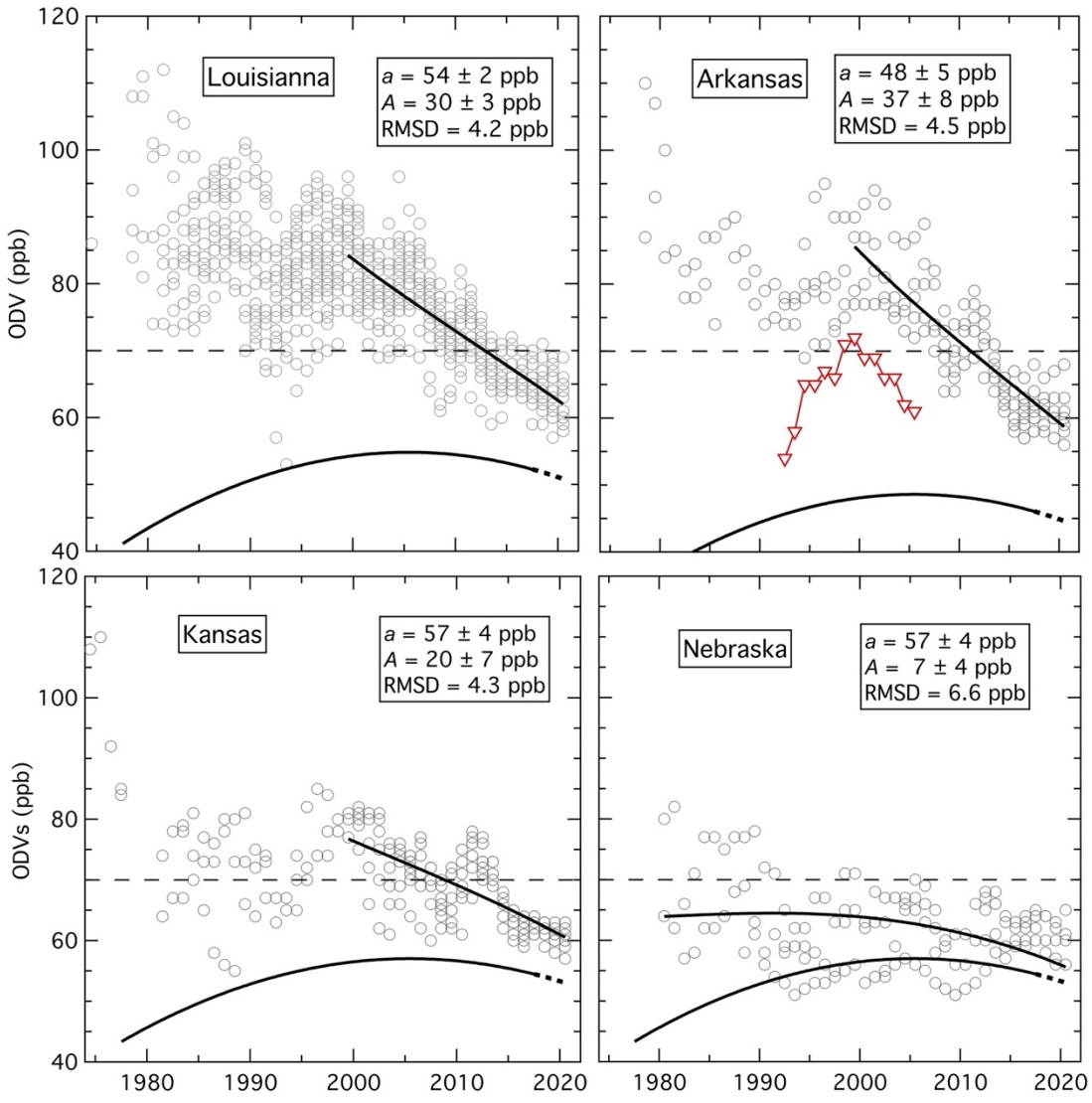

Figure S5. Analysis of time series of ODVs recorded in four neighboring states. Grey symbols in each graph indicate all recorded ODVs in the states. Upper curves indicate fits of Equation 3 to all ODVs in the respective states. The parameters derived in these fits are annotated. Lower curves with dashed extensions indicate the fit to the baseline data from Figure 1, normalized to the respective *a* parameter values. Colored symbols in Arkansas indicate the ODVs from a single site that appear to be outliers, and are excluded from the fit.

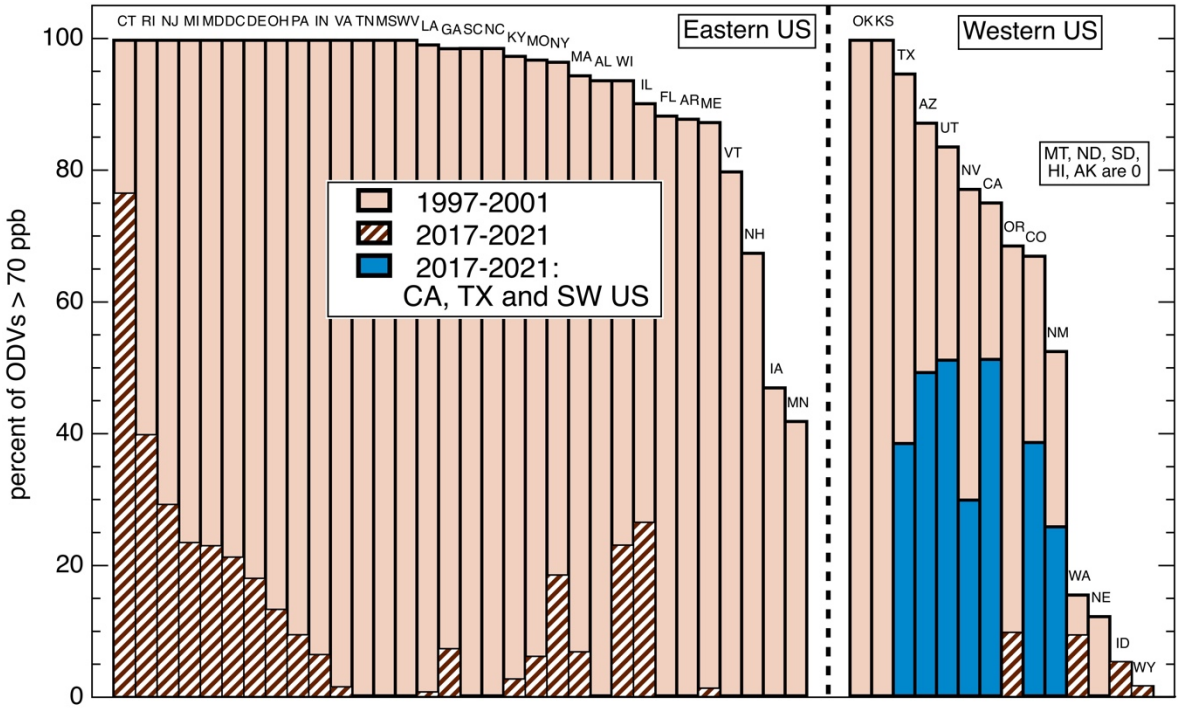

Figure S6. Comparison of percentage of ODVs greater than 70 ppb recorded at all sites in individual states over two 5-year periods: 2017-2021 (hatched and dark blue bars) and a period 20 years earlier - 1997-2001 (light-colored bars). Individual states are indicated by their two letter abbreviations (defined in Table S6). States are arbitrarily divided between eastern and western regions. Southwestern states, Texas and California are indicated by solid dark blue bars. Five states, all in the western region, reported no ODVs greater than 70 ppb. Format is the same as Figure 9 of the manuscript.

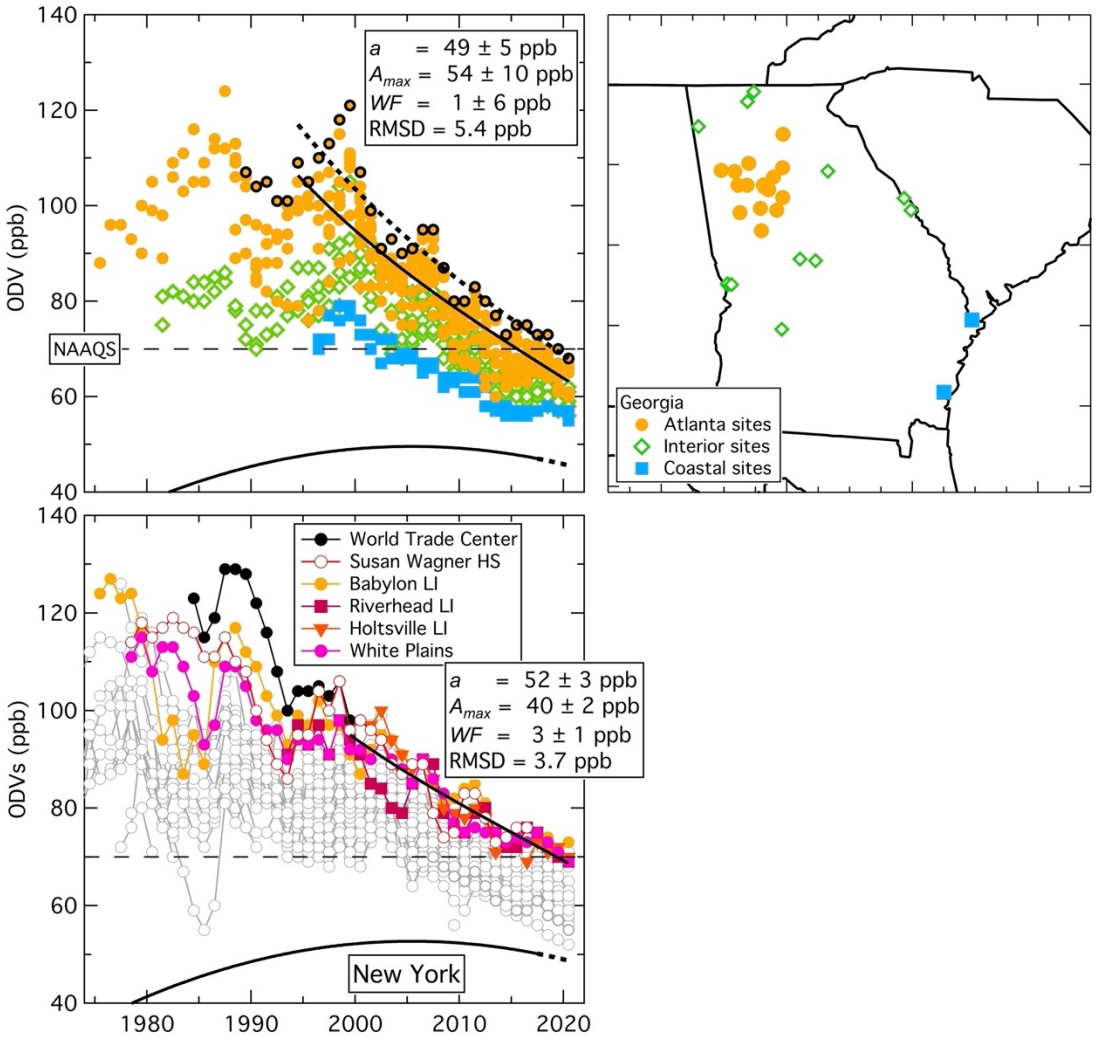

Figure S7. Analysis of time series of ODVs recorded in two eastern urban areas – Atlanta GA and New York City NY. In Georgia ODVs from three groups of sites are indicated with different symbols. Grey symbols in lower graph indicate all recorded ODVs in NY. In the GA graph, upper solid curve indicates fit of Equation 3 to all Atlanta ODVs and the dotted curve indicates fit of Equation 4 to maximum Atlanta ODVs indicated by outlined circles. In NY graph, upper solid curve indicates fit of Equation 4 to the ODVs recorded at the sites representing the maxima in New York City. The parameters derived in the fits to Equation 4 are annotated. Lower curves with dashed extensions indicate the fit to the baseline data from Figure 1, normalized to the respective *a* parameter values. The light dashed lines indicate the 70 ppb ozone NAAQS.

S1. Uncertainty of observation-based and chemical transport model results

Equation 3 provides excellent fits to long-term ozone changes in diverse US regions. As written, Equation 3 has 5 adjustable parameters (*a, b, c, A, τ*); however 3 of these are constants whose values have been determined in previous analyses. Parrish et al. (2020) determined values for $b = 0.20 \pm 0.06$ ppb yr^{-1} and $c = 0.018 \pm 0.006$ ppb yr^{-2} that were the same within derived confidence limits throughout northern midlatitudes. Parrish et al. (2021a) show that these results are consistent with results from 28 published quantifications of changes in average surface ozone concentrations at remote and rural western US locations that are thought to represent background ozone transported into North America. Parrish et al. (2017; 2022) determined a value of $\tau = 21.8 \pm 0.8$ years from the time dependence of ODVs in 7 southern California air basins. This same value (within confidence limits) fit ODV time series throughout the western and northern US (Parrish et al., 2022) and in the northeastern US (Parrish and Ennis, 2019). Substitution of these values for *b, c* and τ into Equation 3 leaves only 2 unknown parameters: *a* and *A*. Section 4 of the paper shows that the resulting Equation 3 with varying *a* and *A* parameter values provides excellent fits to all percentiles of the distributions of the maximum MDA8 ozone concentrations in 4 urban and rural California air basins (Figure 2), and also to ODV time series recorded at rural and remote western US CASTNET sites (Figure 1), at urban and rural sites throughout the southwestern US and Texas (Figures 5, 6 and 8), and in surrounding and more distant US states (Figures S3-S5 and S7). Previous work (Parrish et al, 2017; 2022; Parrish and Ennis, 2019) demonstrate that same equation (or one closely related) provides excellent fits to ODV time series recorded urban and rural sites along the entire US West Coast, in the northern rural states and in the northeastern US.

It is widely accepted that photochemical ozone production involves a very complex set of physical and chemical processes, and that complexity causes ambient ozone concentrations to exhibit a highly non-linear dependence upon precursor concentrations (see e.g., Monks et al., 2015). The excellent fits of a 2 parameter equation to a great number of long-term ozone concentration time series recorded in a widely diverse range of environments demonstrates that there is an underlying simplicity to the evolution of ozone concentrations throughout the US, notwithstanding the complexity of ozone photochemistry. Fully understanding the origins of this simplicity may provide a very useful challenge for CTMs studies.

In previous papers we have discussed inconsistencies between results of observation-based and chemical transport model (CTM) simulations, and among results from different CTM simulations. Section 3.4 and Figure 6 of Parrish et al. (2017) show seven CTM-derived US background ODV estimates for southern California air basins that varied from ~45 to ~65 ppb, with one outlier of 92 ppb; the observational-derived value of 62 ppb agrees well with one of those model results, although it is larger than most others. In their Section 4.2 Parrish and Ennis (2019) compare results from three CTMs with those from our observational-based approach in five US regions; these comparisons show significant spatial correlation between approaches (r^2 values for different CTMs with the observational-based results vary from 0.31 to 0.90), but the CTMs are, on average, systematically lower by 4 to 13 ppb. Zhang et al. (2020) find disagreements of similar magnitude between CTMs; US background ozone estimates from two state-of-the-art global models differed by 5 ppb on average and up to 15 ppb episodically. These disagreements have led to the increasing recognition that CTMs are not yet able to provide accurate estimates of

atmospheric ozone concentrations without incorporating additional information from observations; see, e.g., Skipper et al. (2021) and Hosseinpour et al. (2023).

The following Sections S2-S7 discuss several issues regarding the assumptions and uncertainty of our observation-based approach.

S2. Relationship of US background ODV to ozone exceedance days

(Note: A previous version of some of this material was originally included in the Supplement to Parrish et al., 2022 - https://www.tandfonline.com/doi/suppl/10.1080/10962247.2022.2050962?scroll=top&role=tab)

One important question lacks a definitive answer: Are the four days that record the highest MDA8 ozone concentrations, i.e., the days that determine the ODV at present, the same four days that correspond to the highest US background, i.e., the days that would determine the ODV in the absence of anthropogenic precursor emissions? In other words, do the present highest ozone days also correspond to the days with the largest background ozone? Photochemical models provide a direct answer, but given the uncertainty associated with modeled background ozone concentrations on specific days (estimated as >10 ppb by Jaffe et al., 2018) this answer is likely not reliable. From our observational perspective, we cannot directly answer this question; however observation-based analyses can illuminate this question. It is useful to consider a heuristic example based on artificial data that illustrates some important considerations when considering this issue.

Figure S8 represents an imaginary world that has no meteorological variability; every day is exactly like every other, except that there are gradual seasonal changes. The upper graph shows how MDA8 ozone might vary seasonally at a particular measurement site (black curves decreasing in amplitude over time due to emission controls.) With no US anthropogenic precursor emissions, ozone would equal the US background ozone (blue curve, assumed to average 40 ppb with a sinusoidal variation of 20 ppb amplitude), and would vary smoothly over the year, repeating identically each year. The US background ODV (i.e., the quantity we estimate in our work, which here is assumed constant) would then be given by the blue symbol very near the peak of the blue curve.

US anthropogenic ozone precursor emissions in 2000 are assumed to increase the background ozone by an amount given by the red curve (average 35 ppb with a sinusoidal variation of 40 ppb amplitude). The blue and red curves are 3 months out of phase, in approximate accord with observed Northern Hemisphere background free-tropospheric ozone concentrations that peak in the spring (April/May) and many urban areas that peak in mid to late summer. The total ozone measured in 2000 would then be given by the highest black curve, and the site ODV given by the highest black symbol. Subtraction of the US background ODV from the site ODV gives the US anthropogenic ODV enhancement in 2000 as indicated by the red arrow. Notably, that quantity (60 ppb) is smaller than the US anthropogenic contribution to the ODV in 2000 (~71 ppb, given by orange arrow). This illustration lies at the heart of a common misunderstanding: the US background ODVs reported in this work are not the same as the current contributions of background ozone to current ODVs, because the maxima of background ozone and anthropogenic enhancements are offset from each other in the time of year when they occur. Nevertheless, when considering progress in reducing US anthropogenic precursor emissions, the US background ODV is still germane for considerations of compliance with the NAAQS.

Now we assume that the US anthropogenic ozone production decreases exponentially with a time constant of 20 years. Consequently, the total measured ozone (black curves) decreases year-by-year, with the ODVs (black symbols) also decreasing, and simultaneously shifting to earlier in the year, and approaching the US background ODV (i.e., the blue symbol).

As shown in the lower graph of Figure S8, the changes in site ODVs (black symbols in both graphs) are well fit by an exponential decay, as given by Equation 3 of the manuscript. The derived parameter a = 60.0 ± 0.4 ppb agrees with the 60 ppb maximum of the blue curve, and the parameter A = 59.8 ± 0.3 ppb agrees with the 60 ppb magnitude of the year 2000 US anthropogenic ODV enhancement (red arrow in figure).

An important conclusion from this illustrative example is that confusion can arise if a clear distinction is not made between the US anthropogenic ODV enhancement in 2000 (i.e., the red arrow), the anthropogenic contribution to the site ODV (i.e., the orange arrow) and the anthropogenic ozone production (i.e., the red curve, which varies during the year).

One implication of this example is that episode days (i.e., those exhibiting the highest ozone) in earlier decades are not seasonally coincident with present episode days, and neither of those sets of episode days is seasonally coincident with future episode days. This is due to the growing relative importance of background ozone (which is larger in spring and early summer) as the magnitude of local and regional photochemical production, which is larger later in the summer, decreases. In actuality, episode days in southern California air basins have been observed to systematically move toward the spring from later in the summer; Parrish et al. (2017) show that when monitoring began in the South Coast Air Basin of California (i.e., the Los Angeles urban area) in the early 1970s, the average ozone episode day occurred in late July, but had progressively moved to early July by 2015. This

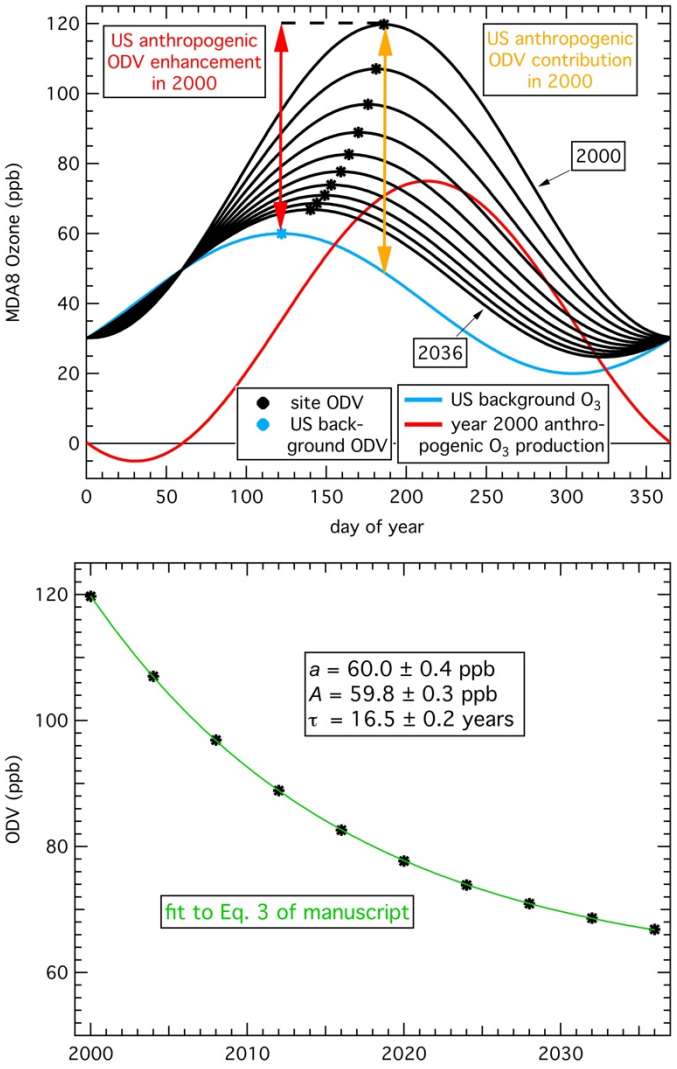

Figure S8: Schematic variation of ozone at a measurement site. **(top)** Blue and red curves give the assumed constant US background ozone and the US anthropogenic ozone production in the year 2000, respectively. The black curves are the total observed ozone in the year 2000 and at progressively later 4-year intervals. The US background ODV is given by the blue symbol, and the site ODVs are given by the black symbols at the peak of their respective curves. The year 2000 US anthropogenic ODV enhancement and anthropogenic ODV contribution are given by the red and orange arrows, respectively. **(bottom)** Temporal evolution of site ODVs from upper graph, fit to Equation 3 of the manuscript, with derived parameters annotated.

seasonal shift of episode days adds considerable uncertainty to photochemical modeling for State Implementation Plan (SIP) development. The meteorological conditions (including the background ozone contribution) on the days that will require the greatest emission control efforts to lower the MDA8 ozone to the NAAQS is uncertain. The common assumption that those days correspond to the present maximum episode days is not valid, since days with higher background ozone concentrations may require even greater emission reductions to reach the NAAQS, even if they now are not the days when the highest ozone is observed.

It should also be noted that an observation-based analysis has indicated a significant positive correlation between maximum observed ozone concentrations and high background ozone concentrations. Parrish et al. (2010) show that MDA8 ozone measured at surface sites in California's Northern Sacramento Valley correlates positively (correlation coefficients as large as +0.53 at valley sites and +0.71 at an elevated surface site) with baseline ozone concentrations measured by sondes launched from the upwind location at Trinidad Head on the northern California coast. This analysis suggests that the days that determine the ODV will progressively tend to be the days of highest US background ozone concentration as anthropogenic ozone contributions are further reduced.

It has been argued (e.g., see Section 1.8 of US EPA, 2020) that the highest US ozone concentrations occur during periods of low background ozone contributions. This argument is based on the reasoning that the largest background ozone contributions occur on spring days with strong convective mixing when ozone generated in the stratosphere or during long-range transport of Asian or natural precursors in the upper troposphere are more readily mixed to the surface. In contrast, the highest US ozone concentrations are thought to occur during multiday episodes under stagnant conditions when an air mass remains stationary over a region abundant in anthropogenic ozone precursor sources. However, this reasoning does not apply to the southwestern US, because surface ozone concentrations are strongly correlated with higher ambient temperatures, and higher temperatures are correlated with deeper atmospheric boundary layers (ABL) in this area. Examination of the climatology of ABL heights over western North America shows that in summer, when most ozone NAAQS violations occur, boundary layers tend to be deepest (see figure 5 of von Engeln and Teixeira, 2013). Deeper boundary layers develop due to greater vertical mixing driven by strong surface heating (i.e., entrainment). A recent paper (Langford et al., 2022) emphasizes that layers with elevated ozone concentrations above Las Vegas were commonly entrained into the ABL and thereby contributed to mean MDA8 regional background ozone concentrations of 50–55 ppb; note that our paper analyzes ODVs, which represent ~98th percentile MDA8 concentrations, and, as expected, the US background ODVs that we quantify are substantially larger than the 50–55 ppb mean background ozone discussed by Langford et al. (2022).

Photochemical modeling in support of air quality policy development has generally focused on days exhibiting the largest MDA8 ozone concentrations. This choice is based on the implicit assumption that such days represent the meteorological conditions under which it will be most difficult to reduce the MDA8 to the NAAQS. Importantly, the US background ODV that is the focus of our analysis may not occur on those same days. Photochemical modeling on days with larger US background ODVs will be very informative, but such days are difficult to specifically identify.

S3. Approximation of long-term change of US anthropogenic ODV enhancements by an exponential decrease

An exponential function is chosen to approximate the long-term decrease of US anthropogenic ODV enhancements because it a) is consistent with our physical understanding of the drivers of urban and rural ozone concentrations, b) is a continuous function, c) is mathematically as simple as possible (i.e., has the fewest possible unknown parameters), and d) successfully accounts for a large fraction of the variance in recorded ODV time series throughout the US.

Any functional form selected for interpretation of an ODV time series must be consistent, first, with a background contribution below which ODVs cannot be reduced by U.S. precursor emission controls alone, and second, with ODVs that have been enhanced above that background due to a pollution contribution, an enhancement that has continually decreased due to decades-long precursor emission reduction efforts. Equation 3 of the manuscript is designed to follow this physical picture. More generally, examination of ozone observations in US urban areas reveals similar trends throughout the country, with general decreases in all areas. A simple intuitive argument suggests that an exponential decrease in the pollution ozone contribution is to be expected. When emission controls are initiated, early progress can be rapid, since there are large emission sources that evolved initially with no plans for their control. As an illustrative example, when emission controls are first initiated it might be possible to reduce the pollution ozone contribution by half in the first 15 years of control efforts. After that period reducing emissions will be harder, since the most easily controlled emissions have been addressed. During the next 15 years, it might be possible to again reduce the remaining pollution ozone contribution by half (i.e., reduction of 25% of the original). A similar argument can be applied to each successive 15-year period. If this example were realistic, then the emission reductions would follow an exponential function, with $\tau = 21.6$ years, close to the value of $\tau = 21.8 \pm 0.8$ years reported by Parrish et al. (2022). Simply put, the expected increasing difficulty of reducing emissions by an absolute amount implies an approximately exponential decrease in the impact of those emissions.

Despite the large variability of tropospheric ozone on a wide spectrum of temporal scales, the underlying long-term changes in ODVs are expected to be continuous, since they are determined by slowly varying drivers such as changes in anthropogenic precursor emissions, land use (which affects natural precursor emissions), and climate. Exceptions might include rapid societal changes, such as occurred during the COVID-19 epidemic response, and volcanic eruptions; however, no discontinuous long-term changes have been encountered in all of the US ODV time series we have analyzed. Thus, the choice of the exponential function, which is continuous, is again indicated.

The exponential term of Equation 3 - $A \exp(-t/\tau)$ - with two parameters is the simplest possible functional form that can capture the behavior of the pollution enhancement. Each ODV is a three-year average; hence a three-decade ODV time series provides only 10 independent data. The ODVs have significant short-term variability (e.g., Guo et al., 2018), so an attempt to quantify systematic, long-term changes from available ODV time series requires fitting to no more than a simple mathematical function for that quantification. That is, to yield precise determinations of the values of the function's parameters the function must have as few unknown parameters as possible. A linear function, also with two parameters - slope and intercept - is often utilized for time series fits; it is as mathematically simple as an exponential function, but a linear fit to a decreasing trend will eventually become negative, and therefore cannot generally be consistent with a positive background contribution. A linear decrease that ends when it

intersects a background function, such as a constant or the function given by the first three terms of Equations 3 and 4 of the manuscript, requires only two parameters, but the resulting function is not continuous. Likewise, piece-wise linear fits are not continuous, and generally require at least four parameters to specify. Any other function that might be applied (e.g., a polynomial fit) would require more than two parameters. From a simplicity and continuity perspective, the chosen exponential function is uniquely suited for quantifying a decreasing ODV time series.

Finally, experience has shown that an exponential function gives excellent fits to the last two to five decades of ozone observed in US urban areas. In their section 2.4 Parrish et al. (2017) present a multivariate fit of Equation 3 (but with a constant background term) to maximum ODV time series in seven southern California air basins over 35 years; the r^2 value for that fit is 0.984. In a similar analysis Parrish and Ennis (2019) find an r^2 value of 0.89 for a shorter (17 year) period of time series of maximum ODVs recorded in eight northeastern states. Section S6 below discusses similar analyses for ODV time series analyzed in this manuscript, and again find large r^2 values – 0.94 for eight Texas regions and 0.79 for the maximum ODV time series in eight southwestern US urban areas. These large r^2 values demonstrate that an exponential function accurately captures a large fraction (approximately equal to the respective r^2 values) of the variance in the ODV time series in all US regions that we have investigated. These considerations demonstrate that an exponential function is a very effective choice for analysis of long-term ozone time series.

S4. Differing rates of decrease of anthropogenic precursor emissions are not directly treated

Equation 3 includes only a single term to account for the influence of decreasing anthropogenic emissions on ODVs; that term depends on a single exponential time constant, τ. However, different anthropogenic emission sectors may have differing time evolution of emissions, which may be expected to be reflected in the temporal evolution of ODVs. In effect, τ in Equation 3 is assumed to represent an average, overall response of ODVs to decreasing anthropogenic emissions.

In this and previous work we discuss the impact of two anthropogenic emission sectors that have not decreased. First, southern California has regions of very intensive agricultural activity - the Imperial Valley in the Salton Sea Air Basin, the San Joaquin Valley Air Basin, and the Salinas Valley in the North Central Coast Air Basin; Parrish et al. (2017; 2022) note that derived a parameter values are biased high by ~ 5 to 12 ppb in these locations, and thus cannot be interpreted as direct determinations of the US background ODV. Second, the development of Equation 4 provides an approximate treatment of the increasing influence of wildfires on ODVs; a small wildfire influence (WF up to 4 ppb) could be discerned in the region studied in this work, and a larger influence (~10-15 ppb) was approximately quantified in urban areas of the Pacific Northwest (Parrish et al., 2022).

There are additional anthropogenic emission sectors that may not have decreased over time, and hence could possibly bias our estimate of US background ODVs. These sources include emissions associated with oil and gas (O&G) exploration, drilling and production, which have increased over the past two decades in some regions of the Western US. In addition, nonroad equipment, such as construction equipment, lawn and garden equipment, and VCP emissions (Coggon et al., 2021) may be important in urban areas, and they have not received as much regulatory attention as anthropogenic emissions. The Supplement Section S5 of Parrish et al. (2022) analyzes time series of

ozone observations in the Bakken O&G basin located in North Dakota, and examines correlations of derived *a* and *A* parameter values in West Coast urban areas. That discussion found no indications of a significant bias arising from these emissions sectors.

S5. Value of exponential decrease time constant, τ, determined in Southern California, applied to the entire southwestern US

We have not found it possible to precisely determine the three parameters (*a, A* and τ) of Equation 3 from a fit to most available US ODV time series. The analysis in the manuscript assumes that τ in the southwestern US and Texas (as well as other states considered) is the same value as derived for southern California ($\tau = 21.8 \pm 0.8$ years). This assumption follows from the perspective of other states closely following the lead of California in emission control efforts, and is supported by the excellent fits provided by Equation 3 to ODV time series throughout the US, as discussed above in Section S4.

Generally, it is not possible to precisely determine the three parameters (*a, A* and τ) of Equation 3 from a fit to most available US ODV time series. Here, however we conduct two iterative, multivariate regression analyses, similar to that described in Section 2.4 of Parrish et al. (2017) and applied by Parrish and Ennis (2019) to the northeastern US. Simultaneous fits to several ODV time series improve the precision of the parameter determinations, allow alternate derivation of some parameter values, and provide alternate estimates of confidence limits for the derived parameter values. Two separate analyses, each analyzing eight ODV time series, are presented. The first analysis fits Equation 3 to ODV time series from the first eight Texas regions listed in Table S5 and illustrated in Figures 8 and S4; the western rural region is omitted due to its small range of recorded ODVs. An ODV time series for each region is obtained by averaging all ODVs collected in that region for each year of the temporal ranges indicated in Table S5. A separate exponential time constant, $\tau_{Ho,}$ is derived for the Houston region, and a single parameter value for τ is derived for the other seven regions. Values of these two τ values and 16 total separate *a* and *A* parameter values for each of the eight regions are optimized in an iterative process that minimizes the sum of the squares of the deviations between the fit and the original mean ODV time series. The second analysis fits Equation 4 to the maximum ODV time series in the seven southwestern US urban areas discussed in Section 4.3 and plotted as light red solid circles in Figures 5 and 6, and the maximum El Paso ODV time series plotted in Figure 8. A similar iterative process attempts to optimize single common parameter values for τ and the wildfire proportionality constant (i.e., the factor of 0.03 in Equation 4) for all areas, and separate *a* and *A* parameter values of each of the eight regions. For both analyses the 18 derived parameter values are given in Table S7, and Figure S9 compares the fits of Equations 3 and 4 to the original ODV time series, both for the original fits discussed in the manuscript (upper graphs) and for the multivariate analyses (lower graphs).

The three derived τ values (18.4 to 19.1 years) are up to 16% smaller than the southern California value of 21.8 ± 0.8 years, and are outside the 95% confidence limit of the California value. However, it is very difficult to force convergence of the Texas multivariate fit, and not possible for the southwestern US analysis due to anti-correlations between parameters. Notably, the agreement between the *a* and *A* parameter values between the original analysis (assuming derived $\tau = 21.8 \pm 0.8$ years) and the multivariate analysis (83% overall) is usually within the confidence

limits of the original analysis, and these multivariate fits provided only very modest improvements over the original fits in the overall r^2 and RMSD values (compare final two rows in Table S7). Given this overall agreement, we are confident in our application of the southern California value of τ throughout the entire region studied in this work.

Table S7. Parameter values derived from multi-variate fits described in Section S3. All units are ppb ozone unless otherwise noted, except for the dimensionless parameter, r^2.

Texas region	**Original fits**[a]	**Multi-var fit**	**SW US urban area**	**Original fits**[b]	**Multi-var fit**[c]
τ (years)	21.8 ± 0.8	18.9 ± 0.9	τ (years)	21.8 ± 0.8	18.4 ± 0.7
τ_{Ho} (years)	21.8 ± 0.8	19.1 ± 2.2	prop. const. ($year^{-1}$)	0.03	0.116 ± 0.19
Dallas - *A*	34.6 ± 4.5	30.3 ± 1.7	Phoenix – A_{WF}	12.9 ± 3.6	12.8 ± 1.9
Dallas - *a*	57.7 ± 3.1	61.6 ± 1.3	Phoenix - *a*	69.0 ± 1.7	70.5 ± 1.7
Houston - *A*	43.2 ± 4.2	39.1 ± 1.7	Tucson - A_{WF}	10.5 ± 1.6	10.6 ± 1.3
Houston - *a*	53.9 ± 3.2	57.9 ± 1.3	Tucson - *a*	63.9 ± 1.4	63.1 ± 1.6
El Paso - *A*	11.5 ± 1.7	9.2 ± 0.6	Las Vegas - A_{WF}	16.1 ± 6.6	16.8 ± 3.3
El Paso - *a*	64.6 ± 1.8	66.6 ± 1.0	Las Vegas - *a*	68.0 ± 2.6	67.6 ± 2.1
San Antonio - *A*	26.6 ± 6.3	25.0 ± 2.2	Reno - A_{WF}	7.0 ± 1.3	6.8 ± 1.2
San Antonio - *a*	58.4 ± 4.1	60.4 ± 1.4	Reno - *a*	66.3 ± 2.2	66.1 ± 1.6
Beau.-PA-LC - *A*	28.0 ± 5.1	25.5 ± 2.2	Salt Lake City - A_{WF}	15.6 ± 2.0	14.9 ± 1.0
Beau.-PA-LC - *a*	54.7 ± 3.4	57.2 ± 1.4	Salt Lake City - *a*	66.6 ± 1.9	66.3 ± 1.5
So Coast Texas - *A*	27.5 ± 6.0	25.6 ± 2.2	Albuquer.-SF - A_{WF}	6.0 ± 1.5	6.9 ± 1.1
So Coast Texas - *a*	52.1 ± 4.1	54.2 ± 1.4	Albuquer.-SF - *a*	66.2 ± 1.8	64.7 ± 1.5
SW Texas - *A*	18.2 ± 6.9	16.7 ± 2.1	Denver - A_{WF}	11.0 ± 1.7	13.4 ± 0.8
SW Texas - *a*	49.8 ± 4.9	51.6 ± 1.4	Denver - *a*	69.0 ± 2.1	64.5 ± 1.5
Tyler-LV-SP - *A*	37.3 ± 6.8	33.8 ± 2.2	El Paso - A_{WF}	14.2 ± 2.1	15.1 ± 0.9
Tyler-LV-SP - *a*	50.8 ± 4.6	54.2 ± 1.4	El Paso - *a*	64.6 ± 1.8	62.3 ± 1.5
r^2 [d]	0.934	0.936	r^2 [d]	0.770	0.794
RMSD [d]	2.65	2.61	RMSD [d]	3.42	3.24

[a] Fits described in Section 4 of the paper. Values are reproduced from Table S5.

[b] Fits described in Section 4 of the paper. Values are reproduced from Tables S3 and S4.

[c] Multivariate fit did not converge; these results were obtained after a large number of iterations of the fitting routine.

[d] r^2 and RMSD are the parameters for the linear regression fit between the actual ODVs and the fit function, as shown in Figure S10.

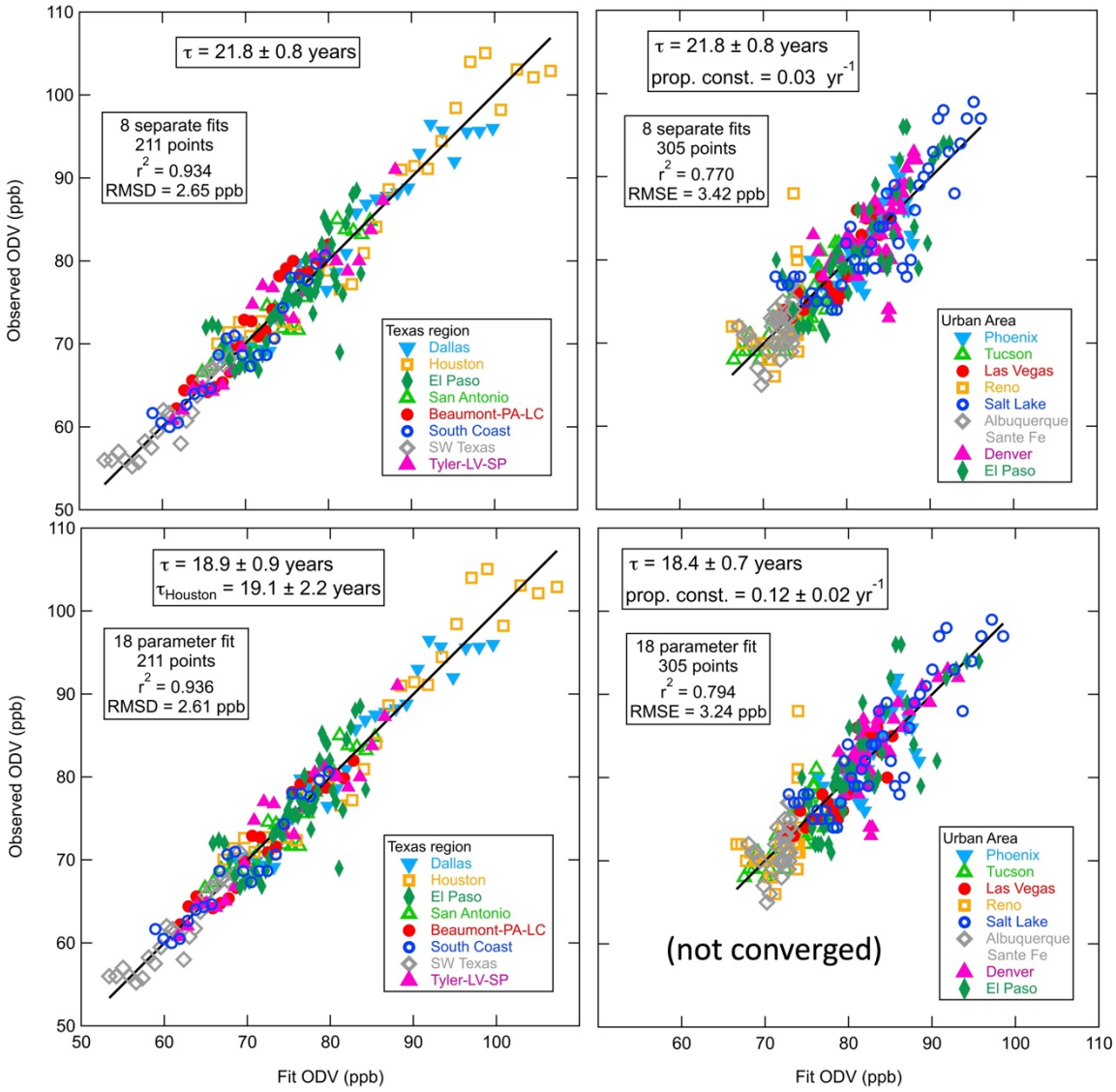

Figure S9. Comparison of observed ODVs with those from fits. The Texas regional and southwestern US urban time series are on the left and right, respectively. The fits to individual time series from the paper are at the top and the simultaneous multivariate fits to all of the time series are at the bottom. Black lines give the linear fit to all points with the intercept held at zero; the slopes of all lines are within 0.0013 of unity, the value expected for a perfect fit. The iterative process was not able to locate a unique minimum for the sum of the squares of the deviations for the 18 parameter fit to the southwestern US urban time series; this is attributed to poor constraints on all 18 parameters in the that data set.

S6. Effect of not considering the US Exceptional Event Rule

In this work we utilize the ODVs tabulated in the data archive of the US EPA to quantify the maximum ozone concentrations impacting surface monitoring sites, and to determine whether a site is approaching or exceeding the NAAQS. It should be noted that if measurement data are influenced by exceptional events, such as wildfires (e.g.,

Jaffe et al., 2013) or stratospheric ozone intrusions (e.g., Langford et al., 2017), those data can, in principle, be removed from the MDA8 monitoring record, as uncontrollable "exceptional events", thereby affecting the ODV archive. More details of the Exceptional Events Rule can be found on the US EPA website: https://www.epa.gov/air-quality-analysis/treatment-air-quality-data-influenced-exceptional-events-homepage-exceptional. If a significant number of ODVs were affected by excluded data, then the ODV archive would not faithfully reflect the actual time series of maximum ozone concentrations, or the true relationship of the ozone concentrations at a site to the NAAQS. Data are excluded when the US EPA concurs with a state's exceptional event demonstration.

The US EPA apparently does not maintain a data base of exceptional event concurrences, but so far as we can determine from an internet search, at the time of this writing, the US EPA has concurred with only one ozone exceptional event demonstration in the western US states examined in this paper since the implementation of the 2016 Exceptional Events Rule. That event was on September 2 and 4, 2017 when wildfires in the Pacific Northwest impacted the National Renewable Energy Laboratory (NREL) ozone monitoring site operated in the greater Denver urban area. As a result of this concurrence the ODV at that site would be reduced by 1 ppb for the years 2017 (from 80 to 79 ppb) and 2019 (from 77 to 76 ppb). In 2017, but not in 2019, this site recorded the maximum ODV in the Denver area, so the urban maximum ODV would be reduced by 1 ppb in 2017, but not affected in 2019. There was a second exceptional event concurrence by the US EPA under an earlier Exceptional Event Rule. That event was on June 14, 2012 when a stratospheric intrusion elevated ozone at two sites in the Upper Green River basin of western Wyoming (State of Wyoming; 2013; Kaldunski et al., 2017) enough that the recorded MDA8 ozone concentrations of 76 and 77 ppb exceeded the 2008 ozone NAAQS.

In summary, archived ODVs can be reduced by US EPA exceptional event concurrences; however, to date concurrences have been extremely limited, and therefore have not significantly affected the analysis presented in this paper. However, future concurrences may possibly affect application of the present analysis approach to coming years.

References not included in manuscript

Coggon, M. M., Gkatzelis, G. I., McDonald, B. C., Gilman, J. B., Schwantes, R. H., Abuhassan, N., Aikin, K. C., Arend, M. F., Berkofff, T. A., Brown, S. S., et al.: Volatile chemical product emissions enhance ozone and modulate urban chemistry, *Proceedings of the National Academy of Sciences* 118 (32):e2026653118. doi:10.1073/pnas.2026653118, 2021.

Guo, J.J., Fiore, A.M., Murray, L.T., Jaffe, D.A., Schnell, J.L., Moore, C.T., and Milly, G.P.: Average versus high surface ozone levels over the continental USA: model bias, background influences, and interannual variability, Atmos. Chem. Phys., 18, 12123–12140, doi.org/10.5194/ac acp-18-12123-2018, 2018.

Jaffe, D., Wigder, N., Downey, N., Pfister, G., Boynard, A., and Reid, S. B.: Impact of Wildfires on Ozone Exceptional Events in the Western US, Environ. Sci. Technol., 47, 11065–11072, https://doi.org/10.1021/es402164f, 2013.

Kaldunski, B., Pierce, R. B., and Holloway, T.: When Stratospheric Ozone Hits Ground-level Regulation: Exceptional Events in Wyoming *Bull. Am. Meteorol. Soc.*, *98*(5), 889-892, doi:10.1175/BAMS-D-14-00133.1, 2017.

Parrish, D. D., Aikin, K. C., Oltmans, S. J., Johnson, B. J., Ives M., and Sweeny, C.: Impact of transported background ozone inflow on summertime air quality in a California ozone exceedance area, *Atmos. Chem. Phys., 10,* 10093–10109, doi:10.5194/acp-10-10093-2010, 2010.

State of Wyoming: Exceptional Event Demonstration Package for the Environmental Protection Agency: Big Piney and Boulder, Wyoming Ozone Standard Exceedances June 14, 2012, edited, Department of Environmental Quality/Air Quality Division, 2013.

US EPA: Integrated Science Assessment (ISA) for Ozone and Related Photochemical Oxidants (Final Report, Apr 2020). U.S. Environmental Protection Agency, Washington, DC, EPA/600/R-20/012, 2020.

von Engeln, A., and Teixeira, J.: A Planetary Boundary Layer Height Climatology Derived from ECMWF Reanalysis Data, J. of Climate, 26(17), 6575–6590, https://doi.org/10.1175/JCLI-D-12-00385.1, 2013.